Application of the vector Monte-Carlo method in polarisation optical coherence tomography

D.Yu. Churmakov, V.L. Kuzmin, I.V. Meglinski

Abstract. The vector Monte-Carlo method is developed and applied to polarisation optical coherence tomography. The basic principles of simulation of the propagation of polarised electromagnetic radiation with a small coherence length are considered under conditions of multiple scattering. The results of numerical simulations for Rayleigh scattering well agree with the Milne solution generalised to the case of an electromagnetic field and with theoretical calculations in the diffusion approximation.

Keywords: polarisation optical low-coherence tomography, Monte-Carlo method, polarisation vector, multiple scattering.

1. Introduction

The visualisation of the internal structure of various objects by nondestructive methods is of primary importance for biological and medical studies. At present optical coherence tomography (OCT) is the most successful and promising method for imaging the internal structure of biological tissues [1 – 5]. The OCT visualisation of the internal structure of biological media proves to be efficient first of all due to the coherent suppression of contribution from multiply scattered photons to a detected optical signal. As a result, the measured interference OCT signal is mainly formed by radiation reflected from interfaces inside a medium and also by photons that have experienced low-order backscattering (less than five – six scatterings). At the same time, multiple scattering (more than 10 scatterings) still considerably restricts OCT applications upon scanning at large depths [6].

The role of multiple and low-order scatterings in the formation of the OCT signal has been studied in many papers [7 – 12]. The results of these studies were used to

D.Yu. Churmakov Cranfield Health, Cranfield University, Silsoe, MK45 4DT, UK; e-mail: d.churmakov@cranfield.ac.uk;
V.L. Kuzmin St. Petersburg Institute of Commerce and Economics, Novorossiiskaya ul. 50, 194021 St. Petersburg, Russia;
e-mail: vladimir.kuzmin@paloma.spbu.ru;
I.V. Meglinski Department of Physics, N.G. Chernyshevskii Saratov State University, Astrakhanskaya ul. 83, 410026 Saratov, Russia; present address: Cranfield University, School of Engineering, Cranfield, MK43 0AL, UK; e-mail: i.meglinski@Cranfield.ac.uk

optimise practical OCT systems and interpret quantitatively the experimental data.

Currently the polarisation methods of optical diagnostics, in particular, polarisation OCT (POCT) find expanding use in the study of biological tissues [3, 13]. Unlike standard OCT, the latter method provides the additional increase in the image contrast of visualised tissues. This probably explains considerable attention given to the development of POCT for applications in non-invasive biomedical diagnostics [14].

The polarisation of probe radiation and its change depend on the type of scattering, which in turn is determined by the size and shape of scattering particles [15 – 17]. Along with scattering, birefringence is also observed during the propagation of polarised light. The polarisation birefringent properties of some biological tissues, for example, collagen (the base of connective tissues) change upon physiological variations and can be used for diagnostics. Thus, POCT was used [18] to study the birefringent properties of biological tissues and their relation with the structure of collagen fibres.

The scattering of electromagnetic radiation in a medium causes a partial depolarisation of radiation and a change in its wavefront [19 – 21]. Because strong anisotropic scattering in the visible and near-IR spectral regions ($\lambda = 400$– 1100 nm, the scattering coefficient $\mu_s \sim 10 - 50$ mm^{-1}, the anisotropy factor $g \sim 0.7 - 0.9$) typical of biological tissues hinders the use of analytic methods for description of the propagation of electromagnetic radiation [2], direct problems are often solved by the Monte-Carlo method (MCM) [7, 11, 12, 22 – 24].

It is assumed that the incident electromagnetic radiation in the diffusion approximation is completely depolarised due to multiple scattering. This means that radiation transfer and associated coherent effects can be described within the framework of a scalar field. Thus, the standard simulation technique of propagation of radiation in random multiply scattering media [11, 12, 22 – 24] is based on the concept of intensity transfer. In this case, phase relations between a pair of fields, whose product gives the intensity, remain beyond the framework of simulations and their consideration requires a special approach.

We showed that the stochastic MCM can be also used to simulate coherent effects of multiple scattering of light in strongly inhomogeneous media. In [25 – 28], the time correlation function of intensity and coherent backscattering was simulated by comparing directly the standard MCM and the iteration solution of the Bethe – Salpeter equation represented as a series in scattering orders. In [29], we con-

sidered a method for simulating coherent effects requiring the consideration of phase shifts such as the time correlation function and interference component of coherent back-scattering. In this paper, we develop this approach for simulating the propagation of polarised electromagnetic radiation with a small coherence length as applied to POCT.

2. Monte-Carlo simulation of polarisation OCT

Optical coherence tomography is based on the principle of low-coherent optical interferometry with the detection of a signal obtained due to the interference of the fields coming from the object and reference arms of a Michelson interferometer [4, 30]. Interference is observed when the difference of optical paths in the object and reference arms does not exceed the coherence length. The amplitude of the detected signal is proportional to the jump of the refractive index at the interface between separate layers or structural elements of tissues located at the depth which corresponds to the optical path in the reference arm. Thus, as in coherence radars [31, 32], it is possible to probe a medium over depth at one aspect angle by determining the position of the jump in the refractive index.

The typical OCT scheme (Fig. 1) includes a Michelson interferometer, a low-coherent source, a scanning optical system (a moving mirror in the simplest case), and a detector. Radiation from the source is split into two beams, one of which being directed to the object arm and the other – to the reference arm. After the propagation of radiation in the medium, the photodetector detects the interference signal obtained upon optical mixing of the reference and object waves. Thus, in the absence of a random medium, when radiation in the object arm is reflected from the mirror, a signal in the photodetector can be written in the form [3, 4]

$$I_{\mathrm{D}}(z) = \langle I_{\mathrm{r}} \rangle + \langle I_{\mathrm{s}} \rangle + 2(\langle I_{\mathrm{r}} \rangle \langle I_{\mathrm{s}} \rangle)^{1/2} \mathrm{Re}[\gamma(\tau)]. \quad (1)$$

Here, $\langle I_{\mathrm{r}} \rangle$ and $\langle I_{\mathrm{s}} \rangle$ are the radiation intensities in the reference and object arms of the interferometer, respectively; the coordinate z describes the displacement of the scanning mirror in the reference arm; $\tau = 2z/c$ is the displacement time of the interfering fields caused by the

Figure 1. Scheme of the typical OCT system: (*1*) light source with a small coherence length; (*2*) photodetector; (*3*) beamsplitter; (*4*) mirror moving at a constant velocity; (*5*) mirror moving with a small amplitude around the rotation axis and performing lateral scan in the sample plane; (*6*) sample; (*7*) reference arm; (*8*) object arm.

additional path difference $2z$; and c is the speed of light in vacuum. The time coherence function $\gamma(\tau) = \gamma(2z/c)$ contains the dependence on the carrier frequency and the emission spectrum of the source [33]. For a radiation source with the Gaussian spectrum,

$$\gamma(\tau) = \exp\left[-\left(\frac{\pi \Delta v \tau}{2(\ln 2)^{1/2}}\right)^2\right] \exp(-2i\pi\bar{v}\tau), \quad (2)$$

where Δv is the FWHM of the emission spectrum of the source and $\bar{v}$ is the carrier frequency of radiation. The coherence length is defined as [4, 30, 33]

$$l_{\mathrm{c}} = \frac{2c \ln 2}{\pi} \frac{1}{\Delta v}. \quad (3)$$

The form of the interference term in Eqn (1) depends on the model of a random medium placed in the object arm of the interferometer. Thus, in the case of a simple model of a sample consisting of weakly reflecting layers, Eqn (1) takes the form [34]

$$I_{\mathrm{D}}(\tau) = \langle I_{\mathrm{r}} \rangle + \langle I_{\mathrm{s}} \rangle + 2(\langle I_{\mathrm{r}} \rangle \langle I_{\mathrm{s}} \rangle)^{1/2} \mathrm{Re}\big\{[R(L_{\mathrm{s}})]^{1/2} \otimes \gamma(\tau_{\mathrm{s}})\big\}, \quad (4)$$

where $R(L_{\mathrm{s}})$ is the fraction of radiation intensity reflected from a layer localised in the sample at the depth L_{s}; $\tau_{\mathrm{s}} = 2(L_{\mathrm{s}} - L_{\mathrm{r}})/c$ is the time delay of a beam reflected from this layer with respect to the reference layer located at a distance of L_{r} from a mirror in the reference arm; and the symbol $\otimes$ denotes the convolution over positions of the layers.

In this paper, we performed Monte-Carlo simulations [24] of the OCT signal by calculating the optical paths of photons propagating in a scattering medium. The contribution of multiple scattering was found as a sum of partial contributions corresponding to each detected photon taking into account the time coherence function (2),

$$I_{\mathrm{OCT}}(\tau) = \sum_{i=1}^{N_{\mathrm{ph}}} W_i \cos\left(\frac{2\pi}{\lambda} \Delta L_i\right)$$

$$\times \exp\left[-4 \lg 2 \left(\frac{\Delta L_i}{l_{\mathrm{c}}}\right)^2\right], \quad (5)$$

where W_i is the statistical weight of the detected photon; ΔL_i is the optical path difference for this photon and a photon in the reference arm; λ is the wavelength of a radiation source in the medium; and N_{ph} is the sampling power. Note that this expression describes the time delay of scattered radiation with respect to the reference signal; after time averaging, it gives rise to an additional stochastic background in the form of speckles.

In the vector Monte-Carlo model, it is necessary to follow additionally variations in the electromagnetic field, which are characterised in our model by the polarisation vector $\boldsymbol{P}$. One of the main advantages of the vector approach compared to the methods based on the calculation of the Stokes–Jones vectors and Mueller–Jones matrices [15, 35–38] is the simplicity of calculations of the components of the polarisation vector at the output from a medium, whose quadratic forms specify the co-polarised and cross-polarised components of the scattered field intensity. Thus, the calculation of the polarisation vector by using the Mueller–Jones matrices after each scattering
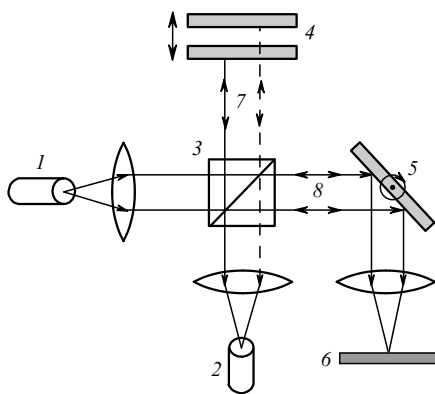
requires cumbersome operations for passing from the global to local coordinate system and vice versa, whereas simulations in the vector model is reduced in fact to the recalculation of the three components of the polarisation vector in the global coordinate system. The simulation of propagation of the polarisation vector in a scattering medium by the vector MCM was proposed for the first time in [27]. Here, we present only the final expression for the calculation of the polarisation vector determined as the result of the action of a chain of operators [29, 39]

$$\left[\hat{I} - \frac{(\boldsymbol{R}_{j+1} - \boldsymbol{R}_j) \times (\boldsymbol{R}_{j+1} - \boldsymbol{R}_j)}{|\boldsymbol{R}_{j+1} - \boldsymbol{R}_j|^2}\right] \qquad (6)$$

on the incident field. Here, $\hat{I}$ is the unit operator; the vectors $\boldsymbol{R}_{j+1}$ and $\boldsymbol{R}_j$ determine the coordinates of successive $j+1$th and jth scattering centres. Tensor operator (6) provides the transverse nature of the electromagnetic field. This operator describes the polarisation of a wave in the far-field approximation (Fraunhofer approximation), which is used in multiple scattering problems when only the long-range component of the field Green function is taken into account.

In the electromagnetic field, except the initial statistical weight, the initial polarisation of the photon field is also specified, which is determined in the general case by three Cartesian coordinates. Let the incident field be polarised along the x axis, then the unit polarisation vector in Cartesian coordinates is parametrised in the form $\boldsymbol{P}_{\text{in}} = (1, 0, 0)$. The coordinates of the polarisation vector change after each scattering event. Therefore, except the usual stochastic determination of the photon direction after a successive scattering event, it is necessary to calculate a new polarisation vector from the previous vector. If a photon packet experiences N scattering events, the polarisation vector at the observation point $\boldsymbol{R}_{\text{D}} = \boldsymbol{R}_{n+1}$ has the form

$$\boldsymbol{P} = \prod_{j=1}^{N} \left[\hat{I} - \frac{(\boldsymbol{R}_{j+1} - \boldsymbol{R}_j) \times (\boldsymbol{R}_{j+1} - \boldsymbol{R}_j)}{|\boldsymbol{R}_{j+1} - \boldsymbol{R}_j|^2}\right] \boldsymbol{P}_{\text{in}}. \qquad (7)$$

After summation over all the detected photon packets N_{ph}, the intensity components of a cw monochromatic wave are written in the form [27]

$$I_{x\alpha} = \sum_{i=1}^{N_{\text{ph}}} W_i P_{i\alpha}^2 \Gamma_{\text{R}}^{N_i}, \qquad (8)$$

where $P_{i\alpha}$ is the modulus of the polarisation vector; $\alpha = \{x, y, z\}$ is the polarisation of observed radiation; N_i is the number of scatterings of the ith photon packet; $\Gamma_{\text{R}} = 2(1 + \cos^2\theta)^{-1}$ is the Rayleigh factor depending on the scattering indicatrix; and $\cos^2\theta$ is the squared scattering angle cosine averaged over the indicatrix. In particular, $\Gamma_{\text{R}} = 3/2$ in the case of scattering by Rayleigh particles of size much smaller than the wavelength and $\Gamma_{\text{R}} \to 1$ in the case of scattering by large particles.

By generalising expression (8) to simulate the contributions of multiple scattering to the OCT signal taking into account the polarisation of the electromagnetic field, we obtain instead of (5)

$$I_{\text{OCT}\alpha}(\tau) = \sum_{i=1}^{N_{\text{ph}}} W_i P_{i\alpha}^2 \Gamma_{\text{R}}^{N_i} \cos\left(\frac{2\pi}{\lambda} \Delta L_i\right) \times$$

$$\times \exp\left[-4 \lg 2 \left(\frac{\Delta L_i}{l_{\text{c}}}\right)^2\right]. \qquad (9)$$

The main contribution to the detected scattered radiation is introduced by photons of low scattering orders at the scan depth where multiple scattering does not dominate yet [6]. We modernised accordingly the scheme of Monte-Carlo simulations to calculate individual contributions of different scattering orders. According to this scheme, the probability of a photon propagating along the trajectory leading directly to a detector from each scattering point (Fig. 2) is calculated before the entry of a photon packet to the detection region determined by the physical dimensions of the detector and its numerical aperture. This detection probability δw_j of the photon packet located at the point P_j is described by the expression

$$\delta w_j = \oiint_{\Omega} p(\boldsymbol{r}) T_{\text{Fr}}(\boldsymbol{rn}) \exp[-(\mu_{\text{s}} + \mu_{\text{a}})|\boldsymbol{r}|] \mathrm{d}\boldsymbol{r}, \qquad (10)$$

where $\boldsymbol{r}$ is the radius vector directed from the point P_j to an element of the detector surface; $p(\boldsymbol{r})$ is the phase function of scattering from the point P_j in the direction $\boldsymbol{r}$; T_{Fr} is the Fresnel transmission coefficient; $|\boldsymbol{r}|$ is the length of the vector $\boldsymbol{r}$; and μ_{a} is the absorption coefficient. The phase function $p(\boldsymbol{r})$ in the integrand describes the probability of scattering at angles within Ω; the exponential $\exp[-(\mu_{\text{s}} + \mu_{\text{a}})|\boldsymbol{r}|]$ is numerically equal to the probability for a photon to pass the path of length $|\boldsymbol{r}|$ without scattering but with possible absorption along the path; and T_{Fr} takes into account refraction at the medium–detector interface. A part of the statistical weight of a photon equal to $W(P_j)\delta w_j$ is detected by the detector; $W(P_j)$ is the photon weight after scattering at the point P_{j-1}. The photon packet continues to propagate according to the standard Monte-Carlo simulation with the statistical weight $W(P_j)(1 - \delta w_j)$. Alternative variants of the semi-analytic approach in Monte-Carlo simulations are discussed in [40] (see also references therein).
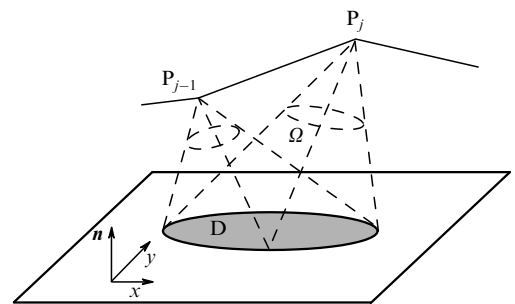

Figure 2. Scheme of Monte-Carlo simulations taking into account the probability of a photon packet scattering towards a detector from each scattering point of its natural trajectory; P_{j-1} and P_j are points of the trajectory of the photon packet scattered inside a medium; D: detector with limited geometrical dimensions and numerical aperture; Ω: solid angle at which the detector is seen from a point of the photon packet trajectory; $\boldsymbol{n}$: normal to the detector surface lying in the simplest case in the xy plane.

3. Simulation results

To demonstrate the possibilities of the proposed polarisation model, we performed numerical simulation for a

semi-infinite medium and a point source. Backscattered radiation is detected with a detector which is infinite in the xy plane and has a small numerical aperture ($\sim 1°$). Figures 3a – c shows the simulation results for the co-polarised and cross-polarised intensity components of backscattered radiation depending on the number of scattering events obtained for three values of the anisotropy factor $g = \overline{\cos \theta} = \{0, 0.5, 0.9\}$ [see (8)]. As expected, after a certain number of scattering events, which depends on g, the co-polarised (I_{xx}) and cross-polarised (I_{xy}) components become almost indiscernible, i.e., radiation is depolarised. In the case of Rayleigh scattering, when $g \approx 0$, the components I_{xx} and I_{xy} are substantially different only up to approximately 10 scattering events, while for $g = 0.9$ – up to 50 scattering events (see Fig. 3).

The depolarisation rate defined as

$$DP = \frac{I_{xx} - I_{xy}}{I_{xx} + I_{xy}} \tag{11}$$

is shown in Fig. 3c for different values of g. For comparison, the depolarisation rate

$$DP = \frac{3(0.7)^{N-1}}{2 + (0.7)^{N-1}} \tag{12}$$

of Rayleigh particles found in the diffusion approximation [39] is also presented. Note that, unlike other polarisation models [15, 35 – 37, 39, 41, 42], in which it is warranted in advance that a sum of the co-polarised and cross-polarised components is equal to the scalar intensity, i.e. $I_{xx} + I_{xy} = I_{scl}$, the fulfilment of equality (12) in our model is provided by the correct consideration of the scattering anisotropy of the electromagnetic radiation, namely, the Rayleigh factor Γ_R.

Monte-Carlo simulations of the POCT signal envelope $I_{OCTx}(z)$ [see (9)] for linearly polarised radiation incident on layers of different thickness d are presented in Fig. 4. Each layer is a homogeneous scattering medium. Reflection from the remote boundary of a layer was simulated as reflection from a mirror with the reflection coefficient $R = 1$ idealising the reflecting surface inside biological tissues. The optical parameters of the medium were calculated for microspheres of diameter 750 nm with the refraction index 1.59 immersed in an aqueous solution. The radiation wavelength was 810 nm and the coherence length l_c of the source in vacuum was 34 μm. The concentration of microspheres was selected to obtain the scattering coefficient μ_s equal to 6.2 mm^{-1}. The rest of the optical parameters of the medium were $\mu_a = 0$ and $n = 1.33$. The anisotropy factor $g = 0.85$ was calculated by using the Mie theory for spheres [21]. The
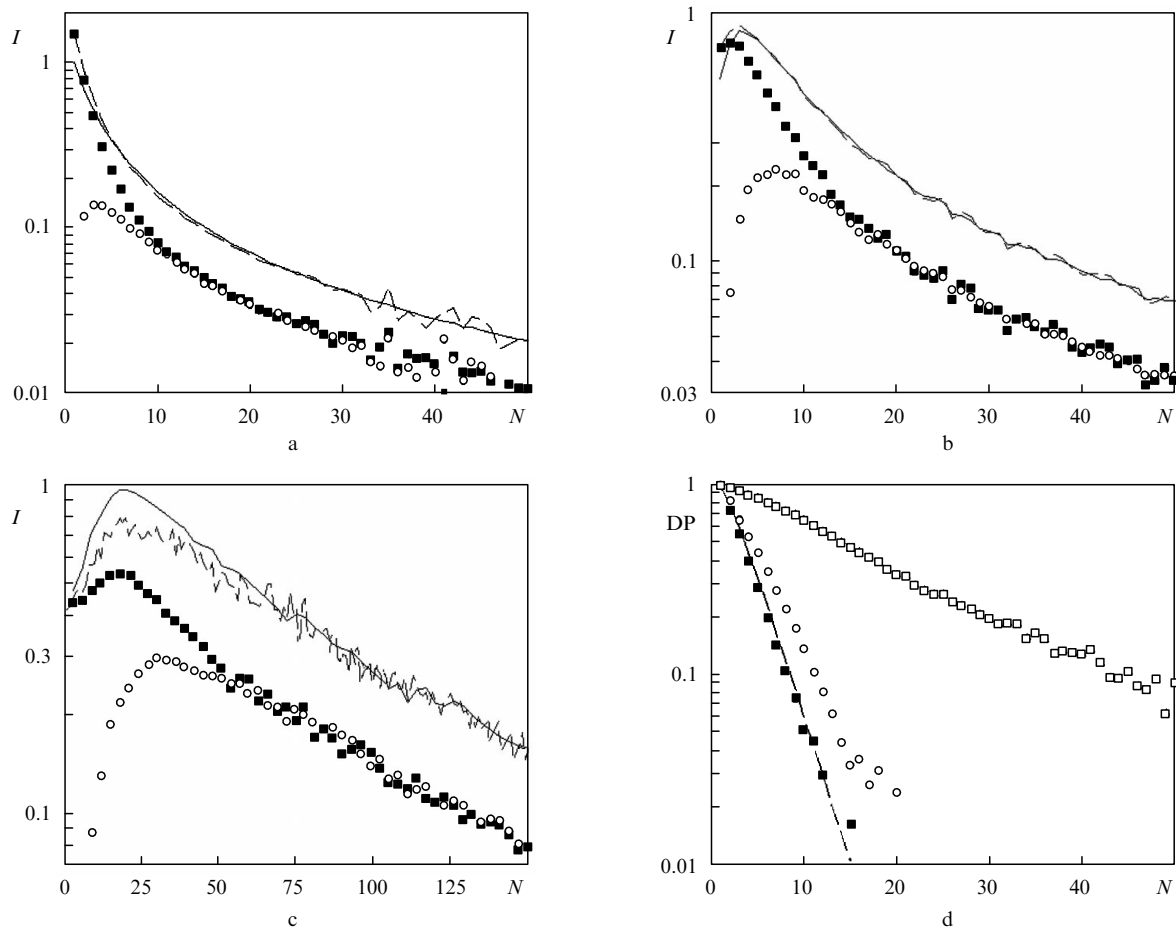

Figure 3. Intensities of multiply scattered linearly polarised radiation normalised to the scalar field intensity as functions of the number of scattering events for the anisotropy factor $g = 0$ (a), 0.5 (b), and 0.9 (c): co-polarised component I_{xx} (■), cross-polarised component I_{xy} (○), scalar field intensity (solid curve), sum $I_{xx} + I_{xy}$ (dashed curve). Depolarisation rate as a function of the number of scattering events for $g = 0$ (■), 0.5 (○), and 0.9 (□); the dashed curve is the depolarisation rate for Rayleigh particles [39] (d). Detection was performed with a small aperture ($\sim 1°$), so that $I_{xz} = 0$. Optical parameters of the medium: $\mu_s = 30$ mm^{-1}, $\mu_a = 0$, the refractive index $n = 1$.

thicknesses d of the scattering layer were selected to obtain optical densities $OD = 2d\mu_s$ equal to 2, 8, and 12, which gives $d = 161$, 650, and 1000 μm, respectively. Scattering was simulated by using the Mie phase function. Photons emitted by a point source are normally incident on the air–layer interface. The diameter of a detector with the numerical aperture corresponding to the angle 14.5° is 420 μm. The optical parameters, size and geometry of the source correspond to the parameters of the experimental setup being developed. The values of parameters are also consistent with those used in other papers [7, 8]. The simulation time was varied from 20 min to a few hours depending on the optical parameters of the medium and the source–detector configuration. Simulations were performed for 2.5×10^6 photon packets by using a 1.8-GHz AMD Sempron 3100 + PC. Note that we developed the simulation algorithm specially intended for PCs commonly used in laboratories.

All the envelopes were normalised to the peak intensity of the POCT signal from the remote boundary. In the case of a small optical density (OD = 2), a signal of double reflection from the remote boundary was observed (see Fig. 4a). The presence of a nonzero signal between the near and remote boundaries of the medium for all layer thicknesses under study is caused by the consideration of phase relations between detected photon packets [see (9)]. Note that the averaging of five–six simulation results efficiently suppresses speckles [43]. A signal from the scattering medium, i.e. the signal between the maxima of the POCT signal increases with increasing the thickness of the scattering medium layer (see Fig. 4) because, as the optical thickness increases, the higher scattering orders begin to contribute to the detected signal (Fig. 5).

To elucidate the influence of multiple scattering on the POCT signal, the reference point of the optical depth of scanning ($z = 0$) was transferred to the point at a distance of the optical path of ballistic photons $L_0 = 2nd$. Figure 6 shows that the fraction of high scattering orders increases with increasing layer thickness; this causes the broadening of a signal reflected from the surface, resulting in a decrease in the axial resolution of a tomograph. Similar results were obtained in papers [7, 8, 44] where alternative simulation methods were used.

Figure 7a presents simulations of scalar OCT and POCT signals for a layer with the optical density OD = 12. Note that the scalar OCT signal I_{OCT} and the co-polarised component I_{OCTx} of the POCT signal do not strongly differ from each other over the entire range of the optical scan depth, except the region $z \geqslant 1330$ μm where the scalar OCT signal exceeds the POCT signal. In this region, the coherent component of the detected signal makes a substantial contribution, i.e. photons that have experienced at least one reflection from the remote boundary and (or) several scattering events. The use of POCT allows one to increase the sampling of a coherent signal from the total multiply scattered detected radiation (Fig. 7a). It should be emphasised that the model of a medium used in our simulations neglects birefringence. For the values of optical parameters that we used ($\mu_s = 6.2$ mm^{-1}, $g = 0.85$), the average number of photon scatterings does not exceed ten even for the maximum thickness of a layer $d = 1000$ μm. Under these conditions, radiation is not completely depolarised yet, as shown in Figs 3c, d, which explains a small difference between the POCT and OCT signals for low scattering
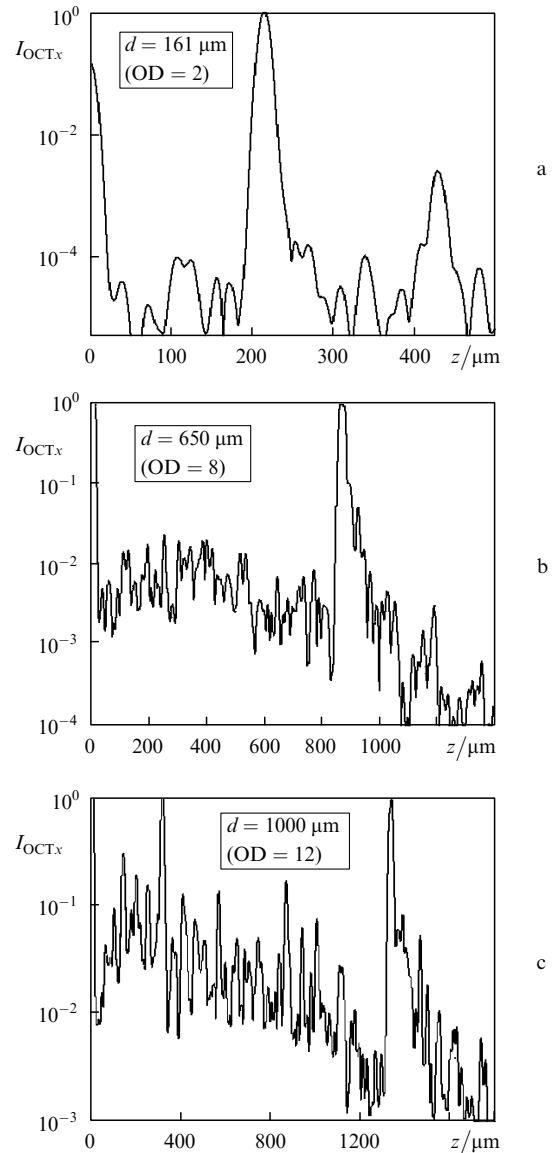

Figure 4. Normalised envelopes of the POCT signal calculated by the MCM for linearly polarised incident radiation as functions of the optical scan depth z for different thicknesses d and optical densities OD of a layer. The optical parameters of the medium: $\mu_s = 6.2$ mm^{-1}, $\mu_a = 0$, $g = 0.85$, $n = 1.33$.
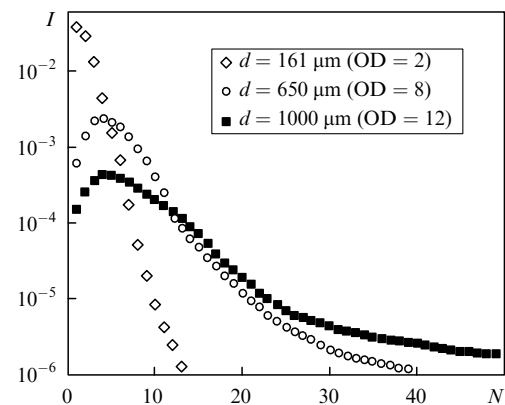

Figure 5. Intensity of the detected backscattered radiation as a function of the number of scattering events for different thicknesses and optical densities of a layer. The optical parameters of the medium are as Fig. 4.
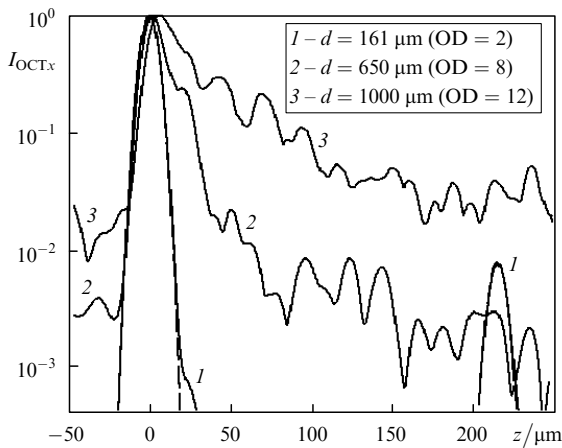
Figure 6. Normalised envelopes of the POCT signal calculated by the MCM for linearly polarised incident radiation as functions of the optical scan depth z for the same thicknesses and optical densities and optical parameters of the medium as in Figs 4 and 5.

orders. The co-polarised and cross-polarised components of the POCT signal for a layer with the optical density OD = 12 are presented in Fig. 7b. The absolute value of
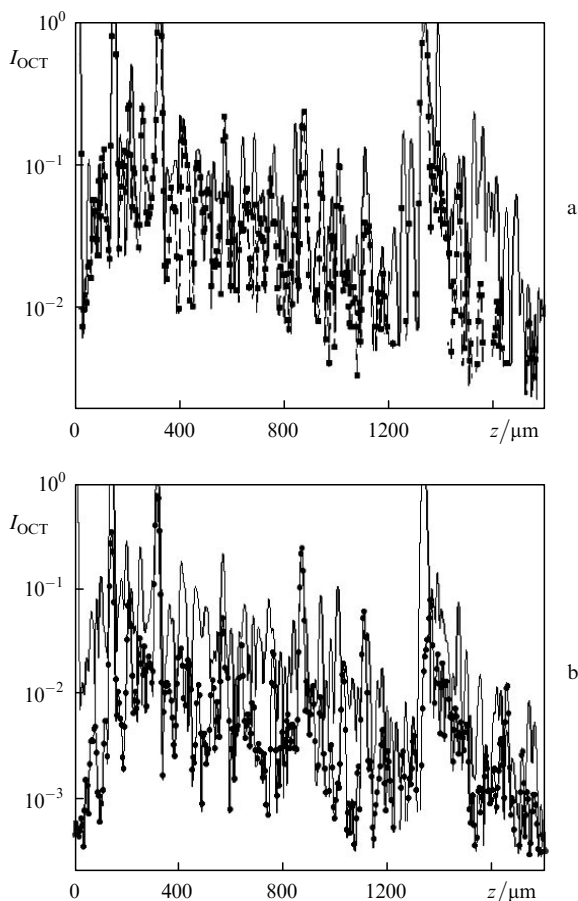

Figure 7. Normalised scalar OCT and POCT signals calculated by the MCM for linearly polarised incident radiation as functions of the optical scan depth z for a layer with the optical density OD = 12: the scalar OCT signal I_{OCT} (solid curve) [see (5)] and POCT signal I_{OCTx} (■) (a), the POCT signal I_{OCTx} (solid curve) and POCT signal I_{OCTy} (●) (b). The optical parameters of the medium: $\mu_s = 6.2$ mm^{-1}, $\mu_a = 0$, $g = 0.85$, $n = 1.33$, $d = 1000$ μm.

I_{OCTy} is smaller than the corresponding value of I_{OCTx} due to a small depolarisation rate, as mentioned above. Note that the maximum of I_{OCTy} is located approximately 30 μm deeper than the real position of the reflecting surface, while the maximum of I_{OCTx} is displaced only by 10 μm. Because the coherence length of the source is $l_c = 34$ μm in vacuum and 25.6 μm in aqueous solution, both these displacements can be neglected.

4. Conclusions

We have considered for the first time the vector method for simulating the propagation of polarised electromagnetic radiation with a small coherence length for applications in POCT. The Monte-Carlo method uses the stochastic model of coherent effects of multiple light scattering based on a direct comparison with the iteration approach to the solution of the Bethe–Salpeter equation [27].

The model proposed in the paper well describes the axial broadening of the POCT signal reflected from a surface with increasing the optical density of the medium. The model also describes the displacement of the signal maximum from its real position, although it is negligible in the case of low-order scattering. These results well agree with simulations and experiments performed in papers [7, 8, 44]. We plan to develop our model by considering in detail the deviation from a linear decrease of the OCT signal with increasing the scan depth [44, 45] and also by analysing layered media with regions actively changing the polarisation of propagating radiation (birefringence of the medium). This model can be used to determine the experimental parameters of POCT/OCT setups and their resolution in the studies of multiply scattering biological tissues.

References

1. Huang D., Swanson E.A., Lin C.P., Schuman J.S., Stinson W.G., Chang W., Hee M.R., Flotte T., Gregory K., Puliafito C.A., Fujimoto J.G. *Science*, **254**, 1178 (1991).
2. Tuchin I.I. *Lazery i volokonnaya optika v biomeditsinskikh issledovaniyakh* (Lasers and Fibre Optics in Biomedical Studies) (Saratov: Saratov University, 1998).
3. Fercher A.F., Drexler W., Hitzenberger C.K., Lasser T. *Rep. Prog. Phys.*, **66**, 239 (2003).
4. Bouma B.E., Tearney G.J. (Eds) *Handbook of Optical Coherence Tomography* (New York: Marcel Dekker, 2002).
5. Tuchin V.V. *Handbook of Coherent Domain Optical Methods: Biomedical Diagostics, Environment and Material Science* (Dordrecht: Kluwer Acad. Publ., 2004).
6. Yadlowsky M.J., Schmitt J.M., Bonner R.F. *Appl. Opt.*, **43**, 5699 (1995).
7. Karamata B., Laubscher M., Leutenegger M., Bourquin S., Lasser T., Lambelet P. *J. Opt. Soc. Am. A*, **22** (7), 1369 (2005).
8. Karamata B., Laubscher M., Leutenegger M., Bourquin S., Lasser T., Lambelet P. *J. Opt. Soc. Am. A*, **22** (7), 1380 (2005).
9. Bizheva K.K., Siegel A.M., Boas D.A. *Phys. Rev. E*, **58** (6), 7664 (1998).
10. Smithies D.J., Lindmo T., Chen Z., Nelson J.S., Milner T.E. *Phys. Med. Biol.*, **43** (10), 3025 (1998).
11. Wang R.K. *Phys. Med. Biol.*, **22** (47), 2281 (2002).
12. Kirillin M.Yu., Meglinski I.V., Priezzhev A.V. *Kvantovaya Elektron.*, **36**, 247 (2006) [*Quantum Electron.*, **36**, 247 (2006)].

13. de Boer J., Milner T.E., van Gemert M.J.C., Nelson J.S. *Opt. Lett.*, **22**, 934 (1997).

14. Special Section On Tissue Polarimetry. *J. Biomed. Opt.*, **7**, 279 (2002).

15. Hielscher A.H., Mourant J.R., Bigio I.J. *Appl. Opt.*, **36**, 125 (1997).

16. MacKintosh F.C., Zhu J.X., Pine D.J., Weitz D.A. *Phys. Rev. B*, **40** (13), 9342 (1989).

17. Bicout D., Brosseau C., Martinez A.S., Schmitt J.M. *Phys. Rev. E*, **49**, 1767 (1994).

18. Ugryumova N., Attenburrow D.P., Winlove C.P., Matcher S.J. *J. Phys. D: Appl. Phys.*, **38**, 2612 (2005).

19. Ishimaru A. *Wave Propagation and Scattering in Random Media* (New York: Academic Press, 1978) Vols 1,2.

20. Brosseau C. *Fundamentals of Polarized Light: a Statistical Optics Approach* (New York: John Wiley & Sons, 1998).

21. Bohren C.F., Huffman D.R. *Absorption and Scattering of Light by Small Particles* (New York: Wiley, 1983).

22. Yamada Y., Hasegawa H., Tamura M., Nomura Y. *Appl. Opt.*, **30** (31), 4515 (1991).

23. Wang L., Jacques S.L., Zheng L. *Computer Methods and Programs in Biomedicine*, **47** (2), 131 (1995).

24. Churmakov D.Y., Meglinski I.V., Greenhalgh D.A. *Phys. Med. Biol.*, **47** (23), 4271 (2002).

25. Kuzmin V.L., Meglinski I.V. *Pis'ma Zh. Eksp. Teor. Fiz.*, **79**, 139 (2004).

26. Kuzmin V.L., Meglinski I.V. *Opt. Spektrosk.*, **97**, 108 (2004).

27. Kuzmin V.L., Meglinski I.V., Churmakov D.Yu. *Zh. Eksp. Teor. Fiz.*, **128**, 30 (2005).

28. Meglinski I.V., Kuzmin V.L., Churmakov D.Y., Greenhalgh D.A. *Proc. Roy. Soc. A*, **461** (2053), 43 (2005).

29. Kuzmin V.L., Meglinski I.V., Churmakov D.Yu. *Opt. Spektrosk.*, **98**, 653 (2005).

30. Hariharan P. *Optical Interferometry* (San Diego: Academic Press, 2003).

31. Dresel T., Hausler G., Ventzke H. *Appl. Opt.*, **31**, 919 (1992).

32. Carlsson T.E., Nilsson B. *J. Opt.*, **29**, 146 (1998).

33. Goodman J.W. *Statistical Optics* (New York: Wiley-Interscience, 1985).

34. Schmitt J.M. *IEEE J. Sel. Top. Quantum. Electron.*, **5**, 1205 (1999).

35. Bartel S., Hielscher A. *Appl. Opt.*, **39** (10), 1580 (2000).

36. Rakovic M.J., Kattawar G.W., Mehrubeoglu M., Cameron B.D., Wang L.V., Rastegar S., Cote G.L. *Appl. Opt.*, **38**, 3399 (1999).

37. Ramella-Roman J.C., Prahl S.A., Jacques S.L. *Opt. Express*, **13**, 4420 (2005).

38. Gangnus S.V., Matcher S.J., Meglinski I.V. *Laser Phys.*, **14** (6), 886 (2004).

39. Akkermans E., Wolf P.E., Maynard R., Maret G. *J. Phys. France*, **49**, 77 (1988).

40. Tinet E., Avrillier S., Tualle J.M. *J. Opt. Soc. Am. A*, **13**, 1903 (1996).

41. Iwai T., Furukawa H., Asakura T. *Opt. Rev.*, **2**, 413 (1995).

42. Zimnyakov D.A., Sinichkin Y.P. *J. Opt. A: Pure Appl. Opt.*, **2**, 200 (2000).

43. Schmitt J.M. *Phys. Med. Biol.*, **42**, 1427 (1997).

44. Lu Q., Gan X., Gu M., Luo Q. *Appl. Opt.*, **43**, 1628 (2004).

45. Tycho A., Jorgensen T.M., Yura H.T., Andersen P.E. *Appl. Opt.*, **41** (31), 6676 (2002).